

# SDO/AIA Observations of Secondary Waves Generated by Interaction of the 2011 June 7 Global EUV Wave With Solar Coronal Structures

Ting Li<sup>1</sup>, Jun Zhang<sup>1</sup>, Shuhong Yang<sup>1</sup>, Wei Liu<sup>2,3</sup>

## ABSTRACT

We present *SDO/AIA* observations of the interaction of a global EUV wave on 2011 June 7 with active regions (ARs), coronal holes (CHs) and coronal bright structures. The primary global wave has a three-dimensional dome shape, with propagation speeds ranging from 430–780 km s<sup>-1</sup> in different directions. The primary coronal wave runs in front of the expanding loops involved in the CME and its propagation speeds are approximately constant within 10–20 minutes. Upon arrival at an AR on its path, the primary EUV wave apparently disappears and a secondary wave rapidly reemerges 75 Mm within the AR boundary at a similar speed. When the EUV wave encounters a coronal bright structure, an additional wave front appears there and propagates in front of it at a velocity nearly a factor of 2 faster. Reflected waves from a polar CH and a coronal bright structure are observed and propagate fractionally slower than the primary waves. Some of these phenomena can be equally explained by either a wave or non-wave model alone. However, taken together, these observations provide new evidence for the multitudes of global EUV waves, in which a true MHD fast-mode wave or shock propagates in front of an expanding CME bubble.

*Subject headings:* Sun: activity — Sun: corona — Sun: coronal mass ejections (CMEs)— Sun: flares

---

<sup>1</sup>Key Laboratory of Solar Activity, National Astronomical Observatories, Chinese Academy of Sciences, Beijing 100012, China; [liting;zjun;shuhongyang]@nao.cas.cn

<sup>2</sup>Lockheed Martin Solar and Astrophysics Laboratory, Department ADBS, Building 252, 3251 Hanover Street, Palo Alto, CA 94304, USA

<sup>3</sup>W. W. Hansen Experimental Physics Laboratory, Stanford University, Stanford, CA 94305, USA

## 1. Introduction

Propagating global disturbances in the solar corona were first detected by the *Solar and Heliospheric Observatory (SOHO)* Extreme ultraviolet Imaging Telescope (EIT; De-laboudinière et al. 1995; Moses et al. 1997; Thompson et al. 1998) and have since then been commonly called “EIT waves”. However, there has been no satisfactory explanation about the nature of such disturbances. Many authors, such as Wang (2000), Warmuth et al. (2001), and Patsourakos & Vourlidas (2009), proposed that they are truly fast-mode magnetohydrodynamic (MHD) waves, while others (Delannée 2000; Chen et al. 2002; Attrill et al. 2007a, 2007b; Chen & Wu 2011; Schrijver et al. 2011) suggested they are apparent waves related to the opening and restructuring of magnetic field lines caused by a coronal mass ejection (CME). A combination of both true wave and non-wave mechanisms was then proposed to reconcile these disparate models (Zhukov & Auchère 2004; Cohen et al. 2009; Liu et al. 2010; Downs et al. 2011). For recent reviews, we refer to Vršnak & Cliver (2008), Wills-Davey & Attrill (2009), Gallagher & Long (2011) and Zhukov (2011).

Global coronal waves have been observed to interact with various coronal structures (Thompson et al. 1998, 1999; Delannée & Aulanier 1999; Wills-Davey & Thompson 1999; Veronig et al. 2006). They tend to avoid strong magnetic fields in active regions (ARs), stop at or partially penetrate into the boundaries of coronal holes (CHs), and stop near a separatrix between ARs. Stopping at CHs was confirmed by MHD simulations (Wang 2000; Wu et al. 2001). In addition, Ofman & Thompson (2002) found strong reflection and refraction of the primary wave from an AR, as well as secondary waves generated by the dynamic distortion of the AR magnetic field. Due to EIT’s low cadence (12–15 minutes) and TRACE’s small field of view, it was difficult to observationally test such numerical simulations. This situation was partly alleviated with the launch of the *Solar-Terrestrial Relations Observatory (STEREO)*; Kaiser et al. 2008) Extreme Ultraviolet Imagers (EUVI; see Wuelser et al. 2004). It detected the first example of reflection and refraction of coronal waves at CH boundaries (Gopalswamy et al. 2009), which were recently numerically reproduced (Schmidt & Ofman 2010). However, STEREO’s improved, yet relatively low cadence of 2.5 minutes left room for potential ambiguity and led to debates about the validity of this result (Attrill 2010).

The new Atmospheric Imaging Assembly (AIA; Lemen et al. 2011) onboard the *Solar Dynamics Observatory (SDO)*; Schwer et al. 2002) takes full-disk images in 10 (E)UV channels at 1".5 resolution and high cadence of 12 s. It thus offers opportunities to elucidate previous ambiguities about the interaction of a global EUV wave with ARs and CHs. We report here such an example observed by AIA in unprecedented detail.

## 2. Observations and Data Analysis

On 2011 June 7, SDO/AIA observed a spectacular solar eruptive event occurring in NOAA AR 11226 (S22W55). It involved an M2.5 flare, a filament eruption, a CME and a global coronal EUV wave (Figure 1). Among the 10 wavelengths of AIA, the 193, 171, 211 and 335 Å channels clearly show the global EUV wave that has a dome-like shape (see also the wave on 2010 January 17 in Veronig et al. 2010) and we focus on these channels in this study. The wave signature is similar in the three hot channels, 193, 211 and 335 Å, but different in the cooler 171 Å channel. The four channels correspond to different temperatures: 193 Å (Fe XII) at 1.5 MK (with a hot contribution of Fe XXIV at 20 MK and cooler O V at 0.2 MK), 171 Å (Fe IX) at 0.6 MK, 211 Å (Fe XIV) at 2.0 MK and 335 Å (Fe XVI) at 2.5 MK (O’Dwyer et al. 2010; Boerner et al. 2011). The coronal wave was also observed by the EUVI aboard *STEREO A* that was 95° ahead of the Earth (Figure 6c). EUVI observes the chromosphere and corona in four spectral channels (304 Å, 171 Å, 195 Å and 284 Å) out to  $1.7 R_{sun}$  with pixel size of  $1''.6$ .

Here, we use a semi-automatic method (see Podladchikova & Berghmans 2005; Liu et al. 2010) to obtain stack plots from 10° wide sectors on the solar surface (“A” and “C”–“G”, Figure 2). Each data point in stack plots is the average of the pixels within a sector along a circular arc at the same distance from the eruption center (S22W55 for Sectors “A”, “F” and “G”) or the initiation site of secondary waves (N8W50 for Sectors “C”–“E”).

## 3. Results

### 3.1. Erupting Loops and Primary Global Coronal EUV Wave

At 193 Å, a series of erupting loops started to expand at 06:20:00 UT (Figures 3b and 5a; Animation 2). They appear as bright stripes with increasing slopes. A parabolic fit indicates an acceleration of  $86 \text{ m s}^{-2}$  and a final velocity of  $280 \text{ km s}^{-1}$ .

At 06:24:33 UT, the global coronal EUV wave initiated in front of the erupting loops (Figures 1b and c; see the Animations 1 and 2). Seen from the stack plots (Figures 3b and 5a), the spatial separation between the coronal wave and the expanding loops indicates that the former propagates in front of the latter. In Sectors “A” and “F”, the velocities of the wave are respectively  $510$  and  $430 \text{ km s}^{-1}$ , and remain constant over the propagation up to 350 Mm. The 211 and 335 Å observations in Sector “A” are similar to those of 193 Å (Figures 3d and e). However, the wave appears different at cooler 171 Å (Figure 3c). A group of small-scale coronal loops are impacted by the coronal wave and expand with a speed

of  $130 \text{ km s}^{-1}$ . The expansion lasts about 3 minutes and then the loops contract to their initial state. This is a possible indicator of loop oscillations triggered by the passage of the EUV wave.

We also investigate the vertical propagation of the wave dome using a straight slice (“B”; Figures 2 and 3*g*). The initial expansion of the loops is evident in the stack plot. Then it faded away with height due to the steep radial intensity gradient. The onset of the wave in this direction coincides with that of the lateral wave. The upward expansion of the dome has a uniform velocity of  $730 \text{ km s}^{-1}$  projected onto the sky plane within the AIA field of view, which is 1.5 times as fast as its lateral expansion to the north, but comparable to that of its lateral expansion toward the south. Note that the erupting filament material is much slower with a large velocity range from  $80 \text{ km s}^{-1}$  to  $400 \text{ km s}^{-1}$ , qualitatively similar to those of coronal jets (e.g., Liu et al. 2009, their Figure 2(a)). The wave signal along Slice “B” is very weak at  $171 \text{ \AA}$  (Figure 3*h*) and not observed at  $335 \text{ \AA}$  (Figure 3*j*).

### 3.2. Secondary Wave Over AR 11228

At 06:30:19 UT, the dome-shaped wave encountered a coronal bright structure (denoted by “1” in Figure 1*a*) and the circular wave front was deformed (Figure 1*d*). Seen from the stack plot of sector “A” (Figures 3*b-e*), the intensity of the coronal wave decreased rapidly after it passed through the coronal bright structure, with an increased velocity of  $1340 \text{ km s}^{-1}$  (Figure 3*b*).

About 2 minutes later, the weak wave arrived at the boundary of AR 11228 and apparently stopped there (denoted by “2” in Figure 2). Almost simultaneously, a secondary wave appeared about 75 Mm into the boundary, which is 506 Mm from the eruption center (Figure 1*e* and Figures 3*b-e*, see the Animation 2). This wave lasted 7 minutes and the velocity decreased from  $500 \text{ km s}^{-1}$  to  $250 \text{ km s}^{-1}$  at 06:39:07 UT. The secondary wave is different from the primary wave in shape and kinematics. The former shows a clear deceleration, while the latter has a uniform velocity during the majority of its lifetime. At 211 and  $335 \text{ \AA}$ , loop brightening in AR 11228 is observed from 06:32 UT (Figures 3*d* and *e*).

### 3.3. Reflected Waves from Bright Structures and a Polar CH

A reflected wave from the coronal bright structure “1” (Figure 1*a* and Figure 2, see the Animation 2) was observed between 06:33:46 UT and 06:42:10 UT (“R1” in Figures 1*f* and *g*; Figures 3*b-e*). In order to investigate the evolution of the reflected wave, we placed Sectors

“C”–“E” starting at this structure (Figure 2) and obtained their running difference stack plots as shown in Figure 4. Initially, the reflected wavefront propagated at a speed of  $140 \text{ km s}^{-1}$ . At 06:36:10 UT, another wavefront was observed in front of it, and propagated at a greater speed of  $250 \text{ km s}^{-1}$  (Figure 1*f* and Figures 4*e-h*). The former and latter wavefronts form a shape of “bifurcation”. About 3 minutes later, the former wavefront faded below detection. The latter wavefront experienced an evident deflection towards the east, and thus the later stage of the wave can be seen in the stack plots of Sectors “D” and “E”. Then the wave disappeared at 06:42:10 UT.

A similar “bifurcation” was also observed when the primary wave approaches the coronal bright structure “3” (Figures 1*a* and *e*, see the Animation 2). As seen in the stack plot of Sector “F” (Figures 5*a-d*), a new wavefront initiated in front of it at 06:31:31 UT, and propagated at a higher speed ( $v \sim 690 \text{ km s}^{-1}$ ). This new wave front was subsequently deflected at the boundaries of ARs (see the red segments in Figures 1*d, f* and *g*), and its propagating direction changed by  $71^\circ$  in 9 minutes, similar to what was observed by Attrill et al. (2007a) and was interpreted as untwisting motions of a twisted flux rope involved in the CME. 171 observations show the wave front in Sector “F” as darkening instead of brightening (Figure 5*b*), similar to that observed by Wills-Davey & Thompson (1999), Liu et al. (2010), Schrijver et al. (2011) and Ma et al. (2011). This is suggestive of heating above the characteristic temperature (0.6 MK) of the  $171 \text{ \AA}$  passband, as simulated by Downs et al. (2011).

Another reflected wave from a southern polar CH (Figure 1*a*) was also observed at 06:46:09 UT (Figures 1*h* and *i*). Seen from the stack plot of Sector “G” (Figures 5*e-h*), the primary wave propagated in the southward direction with a speed of about  $780 \text{ km s}^{-1}$ . The reflected wave from the boundary of the polar CH had a speed ( $v \sim 430 \text{ km s}^{-1}$ ) lower than that of the primary wave. At 06:51:07 UT, the reflected wave was 320 Mm away from the eruption center, and the velocity decreased to  $110 \text{ km s}^{-1}$ . The reflected wave from the polar CH at  $171 \text{ \AA}$  appears as emission reduction (Figure 5*f*).

### 3.4. Three-dimensional Wave Dome

Based on the observed evolution of the wave dome with *SDO* and *STEREO A*, we constructed an approximate three-dimensional shape of the wave dome. The dome is initially assumed to be a spherical crown which is an opaque shell. Then we adjust the parameters of the spherical crown (radius, height) until the projections seen from the two viewpoints match the observed images. The spherical crowns seen from the *SDO* and *STEREO A* viewpoints are shown in right panels of Figure 6. The height of the spherical crown is nearly 1.5 times

as high as its radius (Figures 6*b*, *d* and *f*). For example, at 06:25:30 UT, the radius of the spherical crown was approximately  $0.34 R_{sun}$  and the height was  $0.51 R_{sun}$ . Its volume was about 3.3% of the solar volume. At 06:28:10 UT, the radius and height increased to  $0.45 R_{sun}$  and  $0.675 R_{sun}$ , respectively, resulting in a volume increase of nearly 2.4 times from 06:25:30 UT.

At 06:25:30 UT, the angle between the axis of the dome and the radial direction of eruption center (S22W55) on the surface was about  $22^\circ$  (Figures 6*b*, *d*). About three minutes later, the axis of the dome was inclined southward by  $15^\circ$  (Figure 6*f*), and approached the radial direction of eruption center. In fact, the dome-shaped wave front propagates faster in the vertical direction than the wave front on the solar surface (Figure 3; Veronig et al. 2010), and the spherical dome evolves gradually into an ellipsoid. Full three-dimensional MHD modeling is required to understand these observations.

#### 4. Summary and Discussion

The SDO/AIA observations of the global coronal EUV wave on 2011 June 7 presented here have revealed several very interesting phenomena:

1. Upon arrival at an AR on its path, the primary EUV wave apparently disappeared and a secondary wave rapidly reemerged 75 Mm within the AR boundary with a similar speed of  $500 \text{ km s}^{-1}$ . We speculate two parallel possibilities to explain this discontinuity of wave propagation:

- (1) The AR coronal loops can be perturbed by the impact of the wave and then generate secondary waves, as found in MHD simulations (Ofman & Thompson 2002). In this case, the signal of impact is expected to propagate as a fast-mode wave within the AR. The short duration from the arrival of the primary wave at the AR boundary to the onset of the secondary wave indicates a high velocity of  $2400 \text{ km s}^{-1}$ , as marked by the green dashed line in Figure 3*b*, which is in line with the AR fast-mode speeds found in observations and simulations (Liu et al. 2011; Ofman & Thompson 2002; Williams et al. 2002). However, because the AR has a strong magnetic field and high plasma density, the propagating fast-mode wave could produce very little density and thus EUV intensity perturbation, likely below detection such that the observed wave appears to vanish in the AR.

- (2) Another possibility involves the interpretation of the EUV wave as a consequence of field line stretching (e.g., Chen et al. 2002, their Figure 4). In this case, the AR lies below a separatrix surface under overlying, larger-scale loops. When the expanding CME pushes these overlying loops, the short AR loops underneath remain unperturbed, leading to the

apparent disappearance of the wave. When the next long field line across the separatrix surface is pushed, a new wave front reappears on the far side of the AR. Because of the short distance between neighboring overlying field line across the separatrix, this can result in a large apparent velocity of  $2400 \text{ km s}^{-1}$ .

2. When the EUV wave encounters a bright coronal structure, i.e., small-scale, local loops (instead of large ARs), a new wave front appears there and propagates in front of it at a velocity nearly a factor of 2 faster (see Figures 4*a-h* and 5*a-d*). This is somewhat different from recent AIA observations of fast wave fronts overtaking slow ones with a factor of 2 difference in their speeds (Liu et al. 2010, their Figure 5), but raises similar questions. If the observed wave fronts are indeed MHD waves, their speeds would be determined by the medium in which they propagate. Thus, the speeds along the same direction would be identical, unless the leading wave has altered the local magnetic field and plasma condition, say by compression (Harra et al. 2011), and thus the characteristic wave speed. Our observations suggest that the latter could be the case here. Another possibility is the line of sight projection of waves at different heights. The faster wave front at the bifurcation could result from an upward deflection by the top portion of the small-scale loops toward greater heights, while the slower wave front could be the refraction of the wave at lower heights around these loops. The increase of Alfvén speed and fast-mode speed with height in the low corona within a few solar radius can thus explain their different propagation speeds. Alternatively, this could also be explained if these waves fronts are associated with the expansion of the CME volume of multiple layers at different speeds.

3. There are clearly signatures of reflected waves from a coronal bright structure and a southern polar CH (Figures 3*b-e*, 4 and 5*e-h*). Compared with earlier STEREO observations of a similar event on 2007 May 19 (Gopalswamy et al. 2009), AIA’s high cadence makes this a stronger case as observational evidence that fast-mode (shock) waves are deflected away from regions of high Alfvén speed and reflected in regions of large Alfvén speed gradients (Uchida et al. 1973; Uchida 1974; Wu et al. 2001; Zhang et al. 2011). In recent MHD simulations, Schmidt & Ofman (2010) suggested that the reflected wave observed by Gopalswamy et al. (2009) was triggered by the magnetic pressure difference between the boundary of the CH and the primary wave, and the excitation of secondary waves in different directions was caused by the induced oscillation of the CH. In this event and the X2.2 flare on 2011 February 15, we find that the reflected waves always propagate fractionally slower than the primary waves, while Gopalswamy et al. (2009) found that the reflected wave in certain directions are faster. In any case, this may suggest that the local plasma condition and thus fast-mode wave speeds are changed upon the passage of the primary wave, as we noted above.

4. We find that the wave has a three-dimensional dome shape, similar to that reported

by Veronig et al. (2010). The upward propagation speed of the dome is  $730 \text{ km s}^{-1}$ , while its lateral expansion speed ranges from  $430$  to  $780 \text{ km s}^{-1}$ , depending on the direction (see also Ma et al. 2009). These speeds, a factor of 2 greater than typical EUV wave speeds of  $200\text{--}400 \text{ km s}^{-1}$  (Klassen et al. 2000; Thompson & Myers 2009), fall in the range of the nonlinear MHD wave/shock category proposed by Warmuth & Mann (2011). In addition, the wave front on the solar surface propagates at nearly constant speeds in front of the expanding loops involved in the CME that accelerates up to  $280 \text{ km s}^{-1}$ . This is consistent with early *STEREO* results (Kienreich et al. 2009 and Patsourakos & Vourlidas 2009), as confirmed with numerical simulations (Cohen et al. 2009). Therefore, our observations suggest that the dome could possibly represent a CME driven shock fronts, as recently images by AIA (Ma et al. 2011).

In summary, we find a variety of phenomena associated with the interaction of the global EUV wave with local coronal structures, including secondary waves from ARs and small coronal loops (bright structures), as well as reflected waves from CHs and coronal loops. Some of these phenomena can be equally explained by either a wave or non-wave model alone. However, taken together, these observations provide new evidence for the multitudes of global EUV waves, in which a true MHD fast-mode wave/shock propagates in front of an expanding CME bubble (e.g., Zhukov & Auchère 2004; Cohen et al. 2009; Liu et al. 2010; Downs et al. 2011).

We acknowledge the SECCHI and AIA for providing data. This work is supported by the National Natural Science Foundations of China (40890161, 11025315, 10921303 and 11003026), the CAS Project KJCX2-YW-T04, the National Basic Research Program of China under grant 2011CB811403, and the Young Researcher Grant of National Astronomical Observatories, Chinese Academy of Sciences. Wei Liu was supported by AIA contract NNG04EA00C.

## REFERENCES

- Attrill, G. D. R., Harra, L. K., van Driel-Gesztelyi, L., & Démoulin, P. 2007a, *ApJ*, 656, L101
- Attrill, G. D. R., Harra, L. K., van Driel-Gesztelyi, L., Démoulin, P., & Wülser, J.-P. 2007b, *Astron. Nachr.*, 328, 760
- Attrill, G. D. R. 2010, *ApJ*, 718, 494
- Boerner, P, et al. 2011, *Sol. Phys.*, DOI: 10.1007/s11207-011-9804-8



- Chen, P. F., Wu, S. T., Shibata, K., & Fang, C. 2002, *ApJ*, 572, L99
- Chen, P. F., & Wu, Y. 2011, *ApJ*, 732, L20
- Cohen, O., Attrill, G. D. R., Manchester, W. B., & Wills-Davey, M. J. 2009, *ApJ*, 705, 587
- Delaboudinière, J.-P., Artzner, G. E., Brunaud, J., et al. 1995, *Sol. Phys.*, 162, 291
- Delannée, C. 2000, *ApJ*, 545, 512
- Delannée, C., & Aulanier, G. 1999, *Sol. Phys.*, 190, 107
- Downs, C., Roussev, I. I., van der Holst, B., Lugaz, N., Sokolov, I. V., & Gombosi, T. I. 2011, *ApJ*, 728, 2
- Gallagher, P. T., & Long, D. M. 2011, *Space Sci. Rev.*, in press
- Gopalswamy, N., et al. 2009, *ApJ*, 691, L123
- Harra, L. K., Sterling, A. C., Gömöry, P., & Veronig, A. 2011, *ApJ*, 737, L4
- Kaiser, M. L., Kucera, T. A., Davila, J. M., St. Cyr, O. C., Guhathakurta, M., & Christian, E. 2008, *Space Sci. Rev.*, 136, 5
- Kienreich, I. W., Temmer, M., & Veronig, A. M. 2009, *ApJ*, 703, L118
- Klassen, A., et al. 2000, *A&AS*, 141, 357 Atmospheric Imaging
- Lemen, J. R., et al. 2011, *Sol. Phys.*, 115
- Liu, W., Berger, T. E., Title, A. M., & Tarbell, T. D. 2009, *ApJ*, 707, L37
- Liu, W., Nitta, N. V., Schrijver C. J., et al. 2010, *ApJ*, 723, L53
- Liu, W., Title, A. M., Zhao, J., Ofman, L., Schrijver, C. J., Aschwanden, M. J., De Pontieu, B., & Tarbell, T. D. 2011, *ApJ*, 736, L13
- Ma, S., Raymond, J. C., Golub, L., Lin, J., Chen, H., Grigis, P., Testa, P., & Long, D. 2011, *ApJ*, 738, 160
- Ma, S., Wills-Davey, M. J., Lin, J., et al. 2009, *ApJ*, 707, 503
- Moses, D., et al. 1997, *Sol. Phys.*, 175, 571
- O’Dwyer, B., Del Zanna, G., Mason, H. E., Weber, M. A., & Tripathi, D. 2010, *A&A*, 521, A21

- Ofman, L., & Thompson, B. J. 2002, *ApJ*, 574, 440
- Patsourakos, S., & Vourlidas, A. 2009, *ApJ*, 700, L182
- Podladchikova, O., & Berghmans, D. 2005, *Sol. Phys.*, 228, 265
- Schmidt, J. M., & Ofman, L. 2010, *ApJ*, 713, 1008
- Schrijver, C. J., Aulanier, G., Title, A. M., Pariat, E., & Delannée, C. 2011, *ApJ*, in press
- Schwer, K., Lilly, R. B., Thompson, B. J., & Brewer, D. A. 2002, AGU Fall Meeting Abstracts, SH21C-01
- Thompson, B. J., Plunkett, S. P., Gurman, J. B., Newmark, J. S., St. Cyr, O. C., & Michels, D. J. 1998, *Geophys. Res. Lett.*, 25, 2465
- Thompson, B. J., et al. 1999, *ApJ*, 517, L151
- Thompson, B. J., & Myers, D. C. 2009, *ApJS*, 183, 225
- Uchida, Y. 1974, *Sol. Phys.*, 39, 431
- Uchida, Y., Altschuler, M. D., & Newkirk, G., Jr. 1973, *Sol. Phys.*, 28, 495
- Veronig, A. M., Muhr, N., Kienreich, I. W., et al. 2010, *ApJ*, 716, L57
- Veronig, A. M., Temmer, M., Vršnak, B., & Thalmann, J. K. 2006, *ApJ*, 647, 1466
- Vršnak, B., & Cliver, E. W. 2008, *Sol. Phys.*, 253, 215
- Wang, Y.-M. 2000, *ApJ*, 543, L89
- Warmuth, A., Vršnak, B., Aurass, H., & Hanslmeier, A. 2001, *ApJ*, 560, L105
- Warmuth, A., & Mann, G. 2011, *A&A*, 532, A151
- Williams, D. R., Mathioudakis, M., Gallagher, P. T., Phillips, K. J. H., McAteer, R. T. J., Keenan, F. P., Rudawy, P., & Katsiyannis, A. C. 2002, *MNRAS*, 336, 747
- Wills-Davey, M. J., & Attrill, G. D. R. 2009, *Space Sci. Rev.*, 149, 325
- Wills-Davey, M. J., & Thompson, B. J. 1999, *Sol. Phys.*, 190, 467
- Wu, S. T., Zheng, H., Wang, S., Thompson, B. J., Plunkett, S. P., Zhao, X. P., & Dryer, M. 2001, *J. Geophys. Res.*, 106, 25089

- Wuelser, J. P., Lemen, J. R., Tarbell, T. D., et al. 2004, *Proc. SPIE*, 5171, 111
- Zhang, Y., Kitai, R., Narukage, N., et al. 2011, *PASJ*, 63, 685
- Zhukov, A. N., & Auchère, F. 2004, *A&A*, 427, 705
- Zhukov, A. N. 2011, *Journal of Atmospheric and Solar-Terrestrial Physics*, 73, 1096

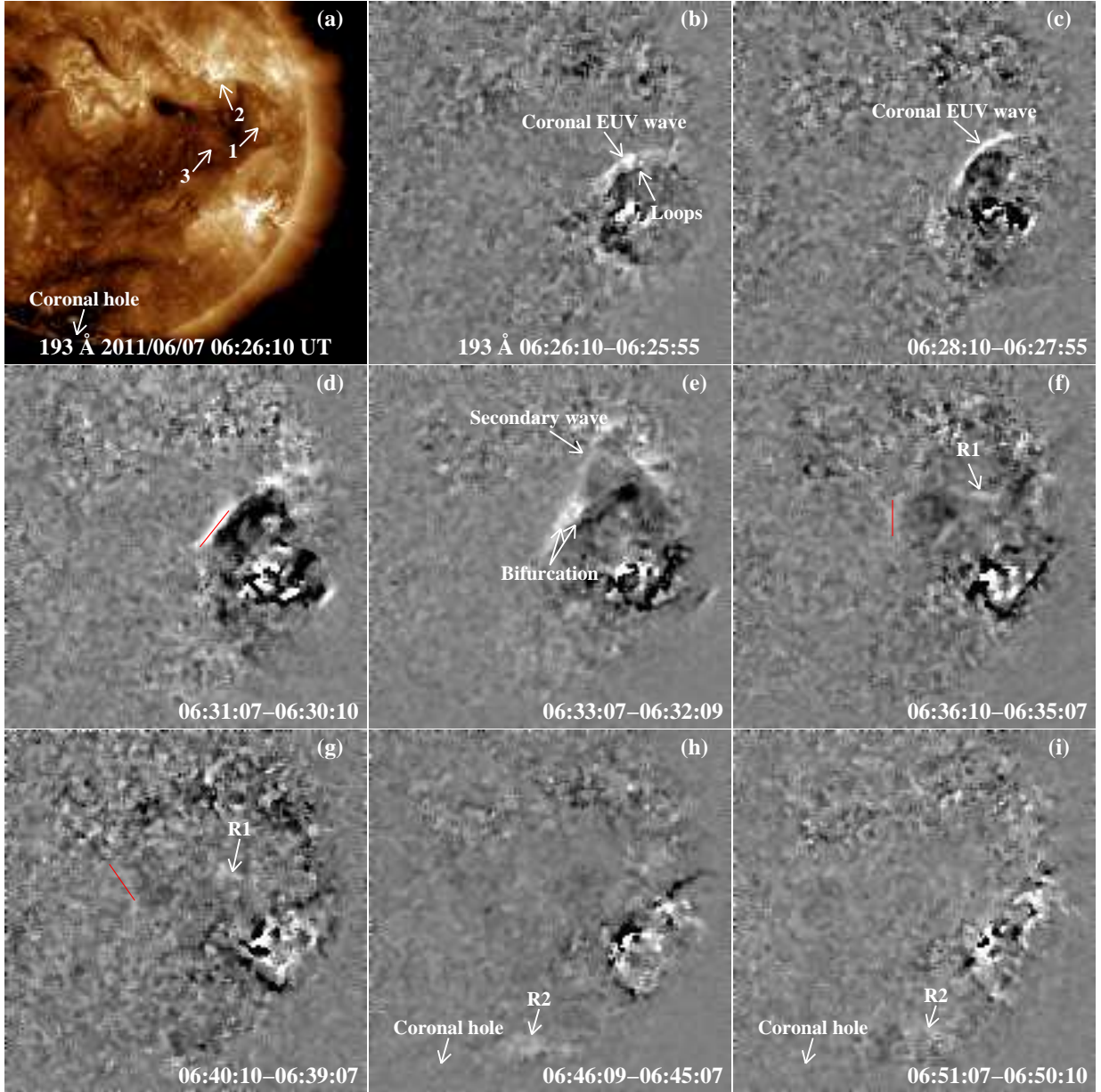


Fig. 1.— *SDO/AIA* 193 Å image (panel *a*, see the Animation 1, available in the online edition of the journal) and running difference images (panels *b–i*, see the Animation 2) showing the evolution of the global coronal EUV wave on 2011 June 7. Arrows “1” and “3” in panel *a* point to two coronal bright structures hit by the coronal wave, and “2” denotes AR 11228. Red lines in panels *d*, *f* and *g* represent the leading edges, indicating the deflection of the wave. “R1” and “R2” denote the reflected waves from the coronal bright structure “1” and from the southern polar CH, respectively.

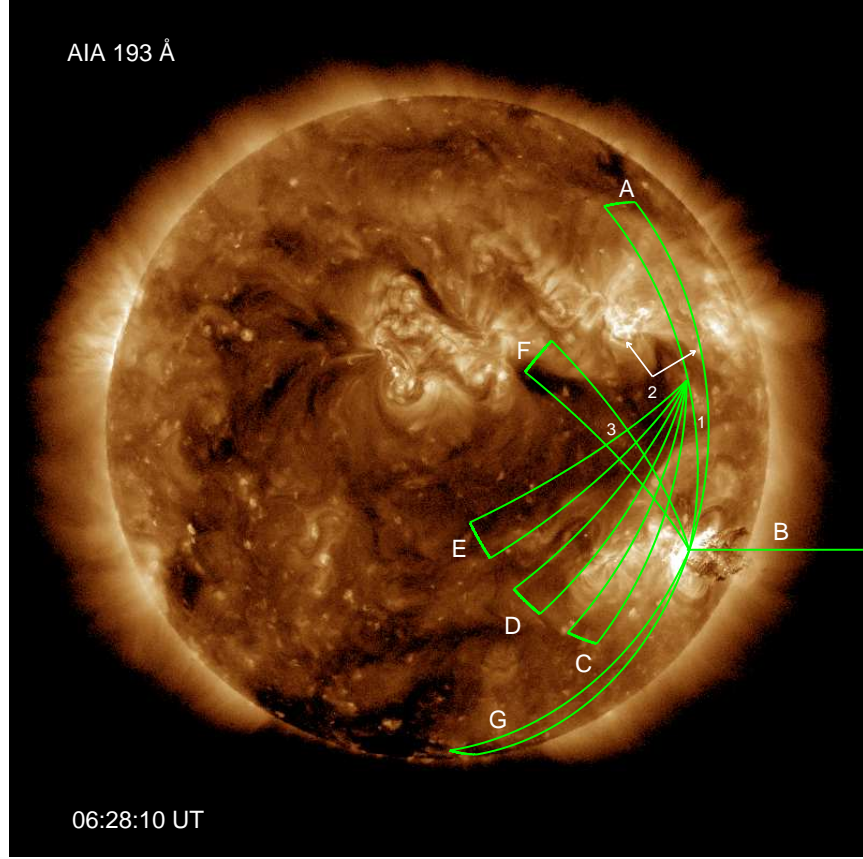


Fig. 2.— *SDO*/AIA 193 Å full-disk image showing six 10° wide sectors (“A” and “C”–“G”) and Slice “B”, which are used to obtain the stack plots shown in Figures 3-5. “1” and “3” denote two coronal bright structures hit by the coronal wave, and “2” represents loop brightenings of AR 11228 (see Figures 3*d* and *e*).



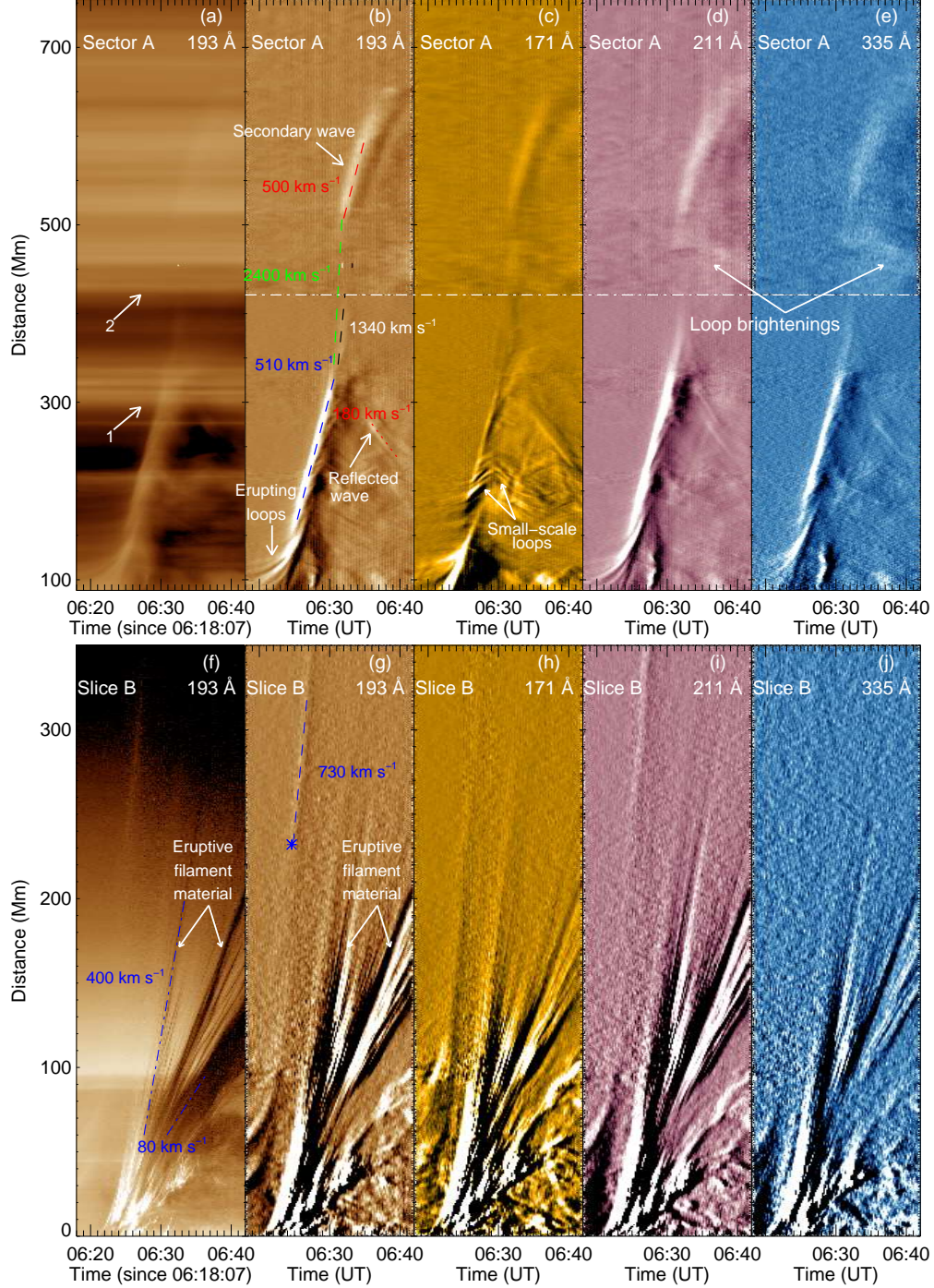


Fig. 3.— Original and running difference stack plots along Sector “A” and slice “B” at 193, 171, 211 and 335 Å. “1” denotes the coronal bright structure hit by the coronal wave and “2” represents AR 11228. In order to visualize the structures better, the images above and below the dash-dotted line are displayed with different color scales. The asterisk in panel *g* marks the start of the wave dome at the limb.

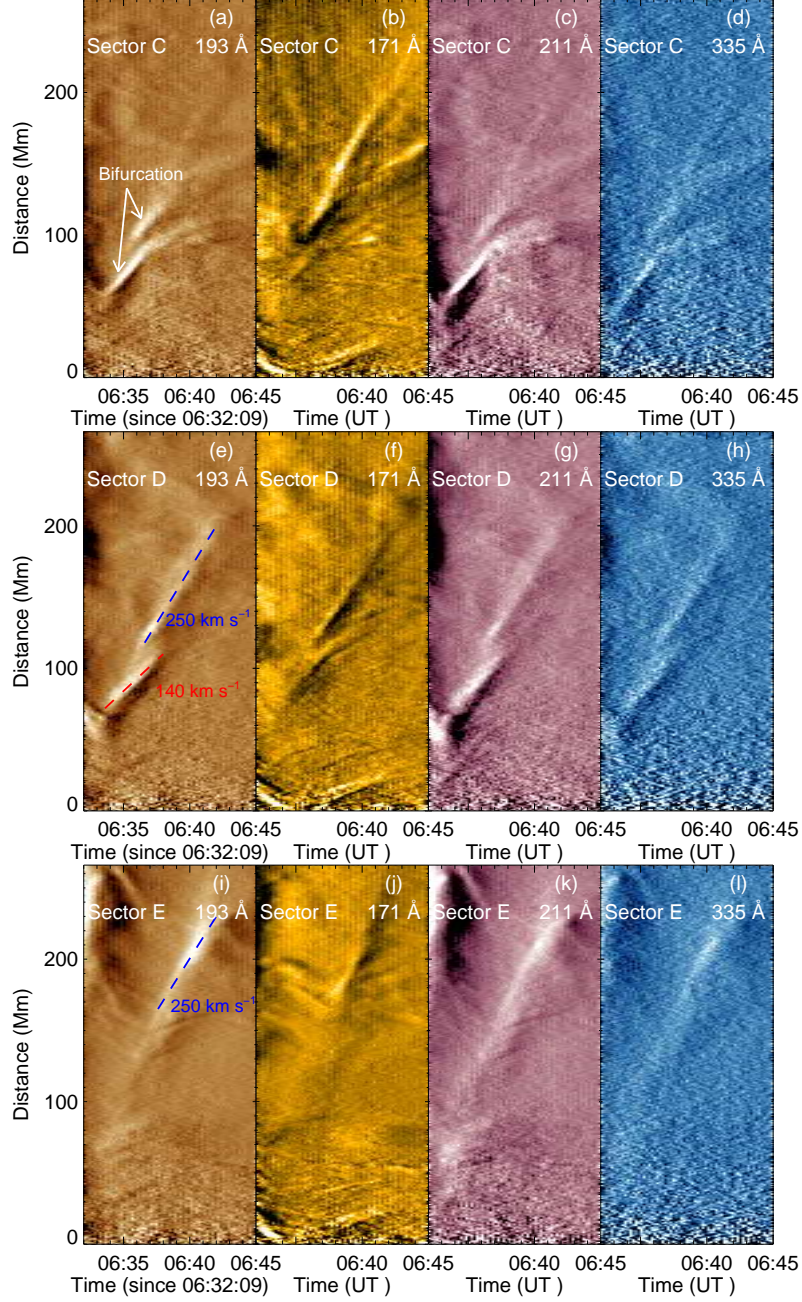


Fig. 4.— Running difference stack plots at 193, 171, 211 and 335 Å along Sector “C” (top panels), “D” (middle panels) and “E” (bottom panels).



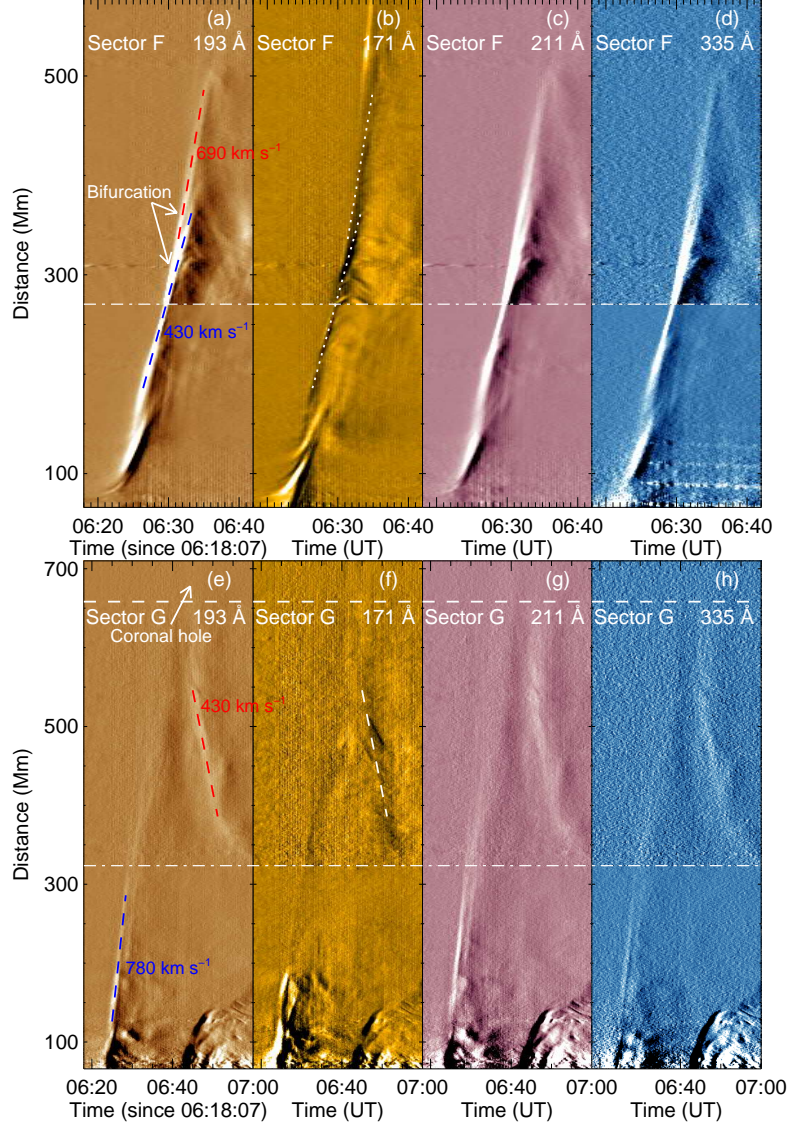


Fig. 5.— Running difference stack plots at 193, 171, 211 and 335 Å along Sector “F” (top panels) and Sector “G” (bottom panels). In order to visualize the structures better, the images above and below the dash-dotted line are displayed with different color scales. The white dashed line in bottom panels represents the boundary of the southern polar CH.



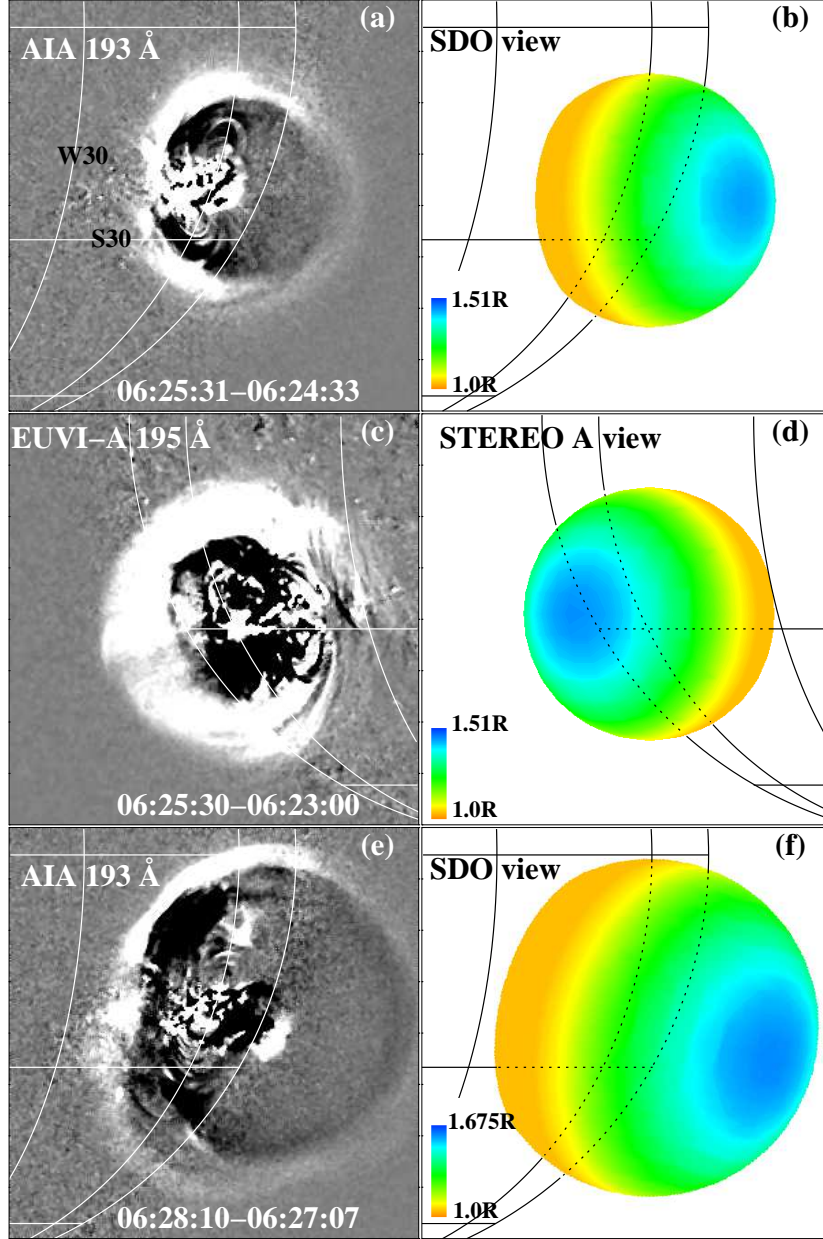


Fig. 6.— Observed running difference images of AIA 193 Å and EUVI-A 195 Å (left panels) and approximate three-dimensional shape of the wave dome (right panels). Color represents height, and “R” denotes the solar radius.